Supporting Information for "Late Pleistocene to Holocene transtension in the northern Cascadia forearc: Evidence from surface ruptures along the Beaufort Range fault"

Emerson M. Lynch[1,2], Christine Regalla[1], Kristin D. Morell[3], Nicolas Harrichhausen[4], and Lucinda J. Leonard[5]

[1]School of Earth and Sustainability, Northern Arizona University, Flagstaff, AZ, USA

[2]Department of Earth and Environmental Geoscience, Washington and Lee University, Lexington, VA, USA

[3]Department of Earth Science, University of California, Santa Barbara, CA, USA

[4]Univ. Grenoble Alpes, Univ. Savoie Mont Blanc, CNRS, IRD, Univ. Gustave Eiffel, ISTErre, 38000 Grenoble, France

[5]School of Earth and Ocean Sciences, University of Victoria, Victoria, BC, Canada

Contents of this file

Additional Supporting Information (Files uploaded separately)

Introduction The Supporting Information contains (1) supporting text outlining criteria used to differentiate tectonic lineaments from those produced by glacial, gravitational, anthropogenic, or differential erosion processes, (2) supporting tables describing surficial units and radiocarbon samples, calculated displacements and slip vectors, and results of kinematic inversions, and (3) supporting figures illustrating tectonic and non-tectonic lineaments, and detailed fault mapping and structural measurements.

Text S1. We differentiated tectonic lineaments (Figure S1) from lineaments that were produced by glacial processes such as glacial scouring, sub-glacial sedimentation (e.g., Figure S2a), and plucking by performing three tests. First, we extracted elevation profiles both along and across scarp crests. While the elevation of crests of glacial lineaments (both erosional and depositional) typically decrease toward the glacial flow direction (down valley, toward 120° azimuth), fault related lineaments can cut across topography following the Rule of 'V's. Second, in the field we evaluated whether glacial and tectonic landforms were underlain by till or had glacially striated or scoured surfaces. Third, while both fault-related scarps and glacially plucked surfaces may have asymmetric profiles across the landform, glacially plucked surfaces face in the ice transport direction (∼120° azimuth), whereas fault-related lineaments primarily face uphill.

We differentiated lineaments that were produced by gravitational failure, such as landslides or sackungen, from tectonic lineaments by considering the context of the deposits around the lineaments. Landslide surfaces are often hummocky and disturbed, whereas fault scarps may offset surfaces of any preservation. Lineaments formed by landslide headscars or "toes" are typically curvilinear, whereas fault-related lineaments are typically linear. Lineaments formed by sackungen (e.g., Figure S2b) typically occur near the top of the range in parallel linear sets, whereas fault-related lineaments can occur at any elevation, often in splay or en echelon geometries, and produce vertical separation of the hillside.

We differentiated lineaments that were produced by anthropogenic disturbance from tectonic lineaments by comparing mapped lineaments with logging roads, timber hauling paths, and damage from heavy machinery on modern and historical air photos and road maps. Lineaments associated with logging roads or paths (e.g., Figure S2c) typically have a flat base with an oversteepening of the lateral flanks from road construction, whereas fault-related lineaments do not.

We tested that mapped scarps were not the result of differential erosion of bedrock faults, bedding, or flow banding from tectonic lineaments using the following criteria. Scarps produced by differential erosion are not associated with vertical separation of the hillside. Vertical separation requires displacement of the ground surface. We also measured the inclination of any Nanaimo Fm. beds and Karmutsen flow tops located near scarps. Lineaments formed by differential erosion are typically co-located with steeply dipping bedding planes (e.g., within the Nanaimo Fm.), whereas fault-related lineaments can occur in beds of any dip magnitude, and do not have to be co-located with or parallel to bedding planes.

Figure S1. Distribution of known and inferred active fault strands along the Beaufort Range fault. These fault-related scarps, sag ponds, and pressure ridges (red and blue lines) occur discontinuously for >60 km along strike and are distinct from those formed through glacial, gravitational, or anthropogenic processes (e.g., Figure S2a-c). Lineaments extend from the Forbidden Plateau in the northwest (the epicenter of the 1946 M 7.3 Vancouver Island earthquake; Rogers and Hasegawa, 1978), through the steep rangefront of the Beaufort Range, and toward the southeast where the Beaufort Range fault projects toward the Cameron River and Fulford faults in Canada. The Fulford fault projects toward the Skipjack Island fault zone in the USA (see Main Text Figure 1 for locations of regional faults). Fault-related scarps are mapped in both the hanging wall and footwall of the Eocene bedrock Beaufort Range fault (bold barbed black line; bedrock geology and faults after Cui et al., 2017), a thrust fault that places Late Triassic Karmutsen Fm. basalts over the Cretaceous Nanaimo Gp. Fault scarps offset Quaternary deposits ranging in age from ∼13.6-11 ka to ∼3-4 ka (see Main Text Figure 4 for surficial mapping).

Table S1. Sediment and surface morphology descriptions of units mapped in Main Text Figure 4.

Table S2. BRF displacements and slip vectors determined from reconstructions of offset geomorphic piercing lines.

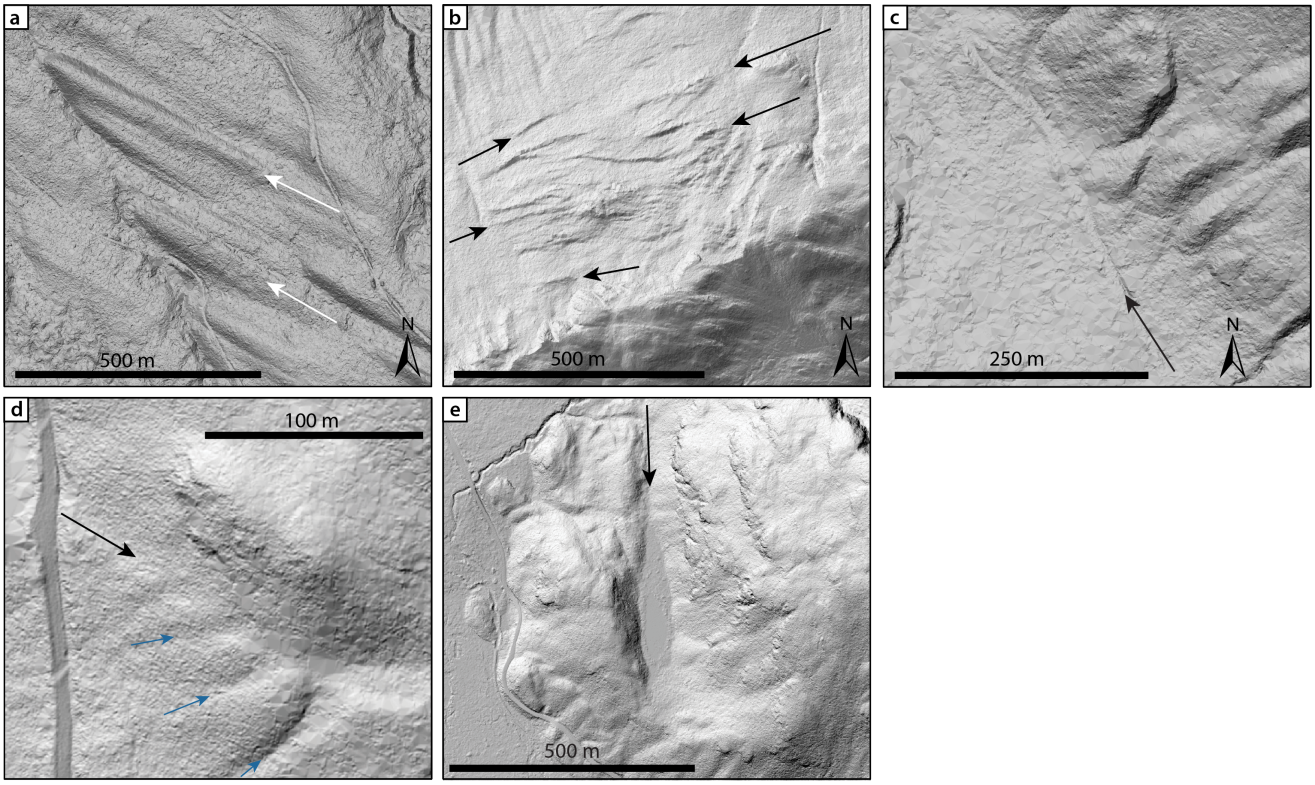

Figure S2. Hillshaded lidar DEMs showing examples of non-tectonic (panels a-c) and tectonic (panels d and e) lineaments along the Beaufort Range. **A:** White arrows indicate streamlined glacial drumlins and lineaments. These lineaments trend down-valley toward ∼120°, sub-parallel to the valley glacier flow direction of Fyles (1963). **B:** Black arrows indicate sackungen, parallel linear scarps near ridge crests associated with gravitational failures after retreat of a glacial buttress (e.g., Li et al., 2010). **C:** Black arrow indicates a decommissioned logging road. The uphill side (right) is carved out, while the downhill side (left) is oversteepened due to deposition of excess material during road building. **D:** Black arrow points to a "bench," or a flat, degraded topographic feature embedded in the high-gradient hillslope, that truncates several paleochannels (blue arrows). **E:** A linear depression developed in Karmutsen Fm. basalt that collects water (a sag pond), the trend of which is oblique to the range front.

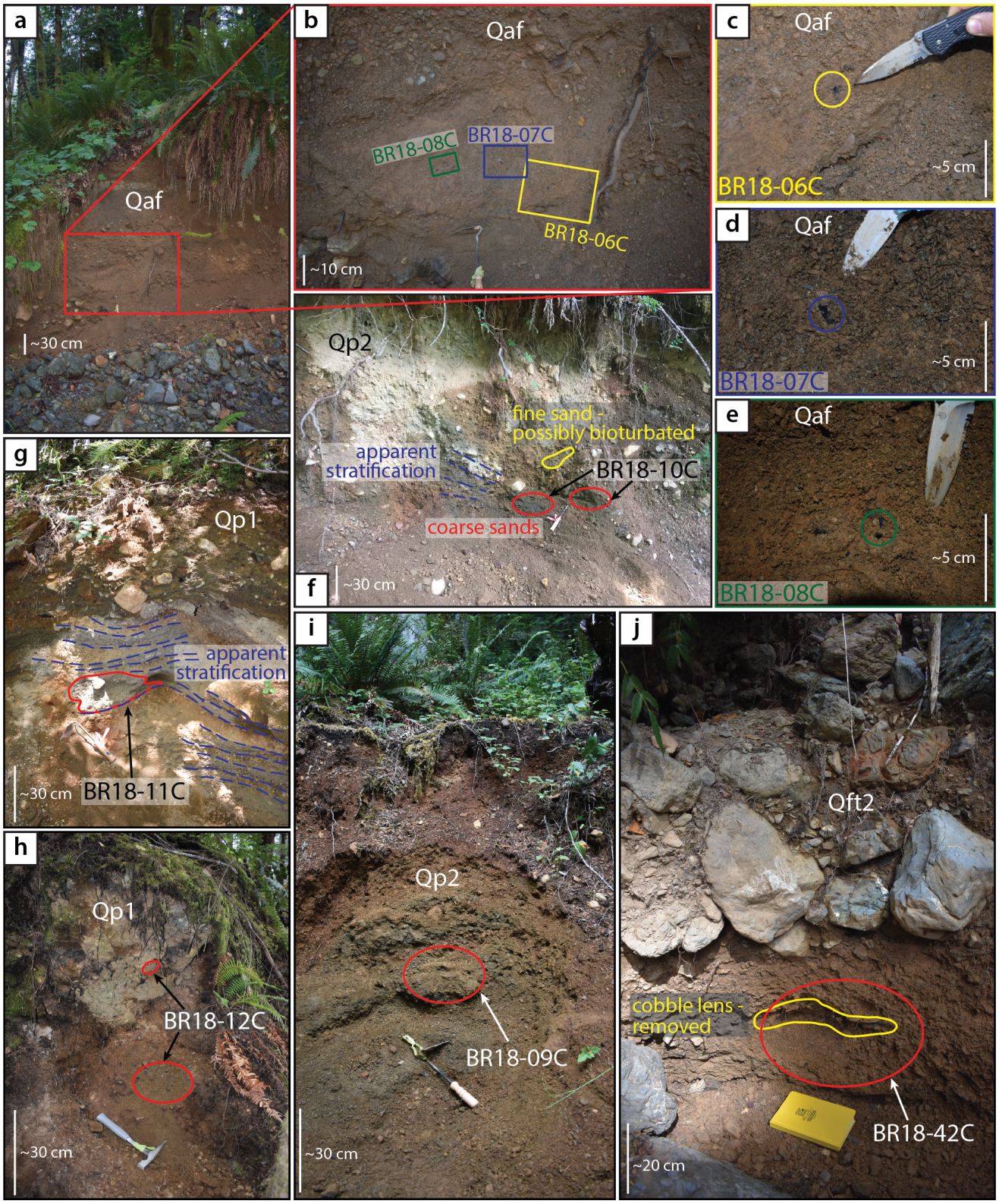

Figure S3. (Caption next page)

Figure S3. (Previous page). Photos of radiocarbon sample locations and surrounding deposits. **A:** Alluvial fan (Qaf) exposure in active stream channel where samples BR18-06C, -07C and -08C were collected. Deposit consists of interbedded cobbles and gravels with some finer sand beds and lenses. Beds are roughly horizontal and clast supported, with sub-angular to sub-rounded clasts. The matrix is similar throughout, red-brown with a muddy composition, likely composed of Fe oxides with clay and sands. The alluvial fan unit is 2-3 m thick and topped by a fluvial deposit, overlain by colluvium. **B:** Close-up of the location in panel A showing the individual sample locations within the Qaf deposit. Samples BR18-06C, -07C, and -08C were collected from a ∼1 m wide by 30-40 cm thick lens of pebbles and coarse sands, ∼1 m above the active channel floor, ∼2 m below the fan surface. **C:** Sample BR18-06C in situ. **D:** Sample BR18-07C in situ. **E:** Sample BR18-08C in situ. **F:** Road cut exposure where sample BR10C was collected from an indurated coarse sand lens (outlined in red) within stratified sands and gravels (Qp2). **G:** Roadside exposure where sample BR18-11C was collected from sandy interbeds outlined in red (Qp1). Colluvium and detritus on the surface was removed, and bulk sediment sample was collected from freshly exposed sediments. **H:** Paraglacial deposit exposure (Qp1) where sample BR18-12C was collected. This deposit was very indurated, and required hammering to collect bulk sediment (area sampled outlined in red). **I:** Roadside exposure where sample BR18-09C was collected. Colluvium and detritus on the surface was removed, and bulk sediment sample was collected from freshly exposed Qp2 sediments (outlined in red). **J:** Fluvial terrace (Qft2) exposure in active stream channel where sample BR18-42C was collected from a pebble bed (outlined in red). The cobble lens indicated in yellow was plucked out prior to sampling due to an abundance of plant litter.

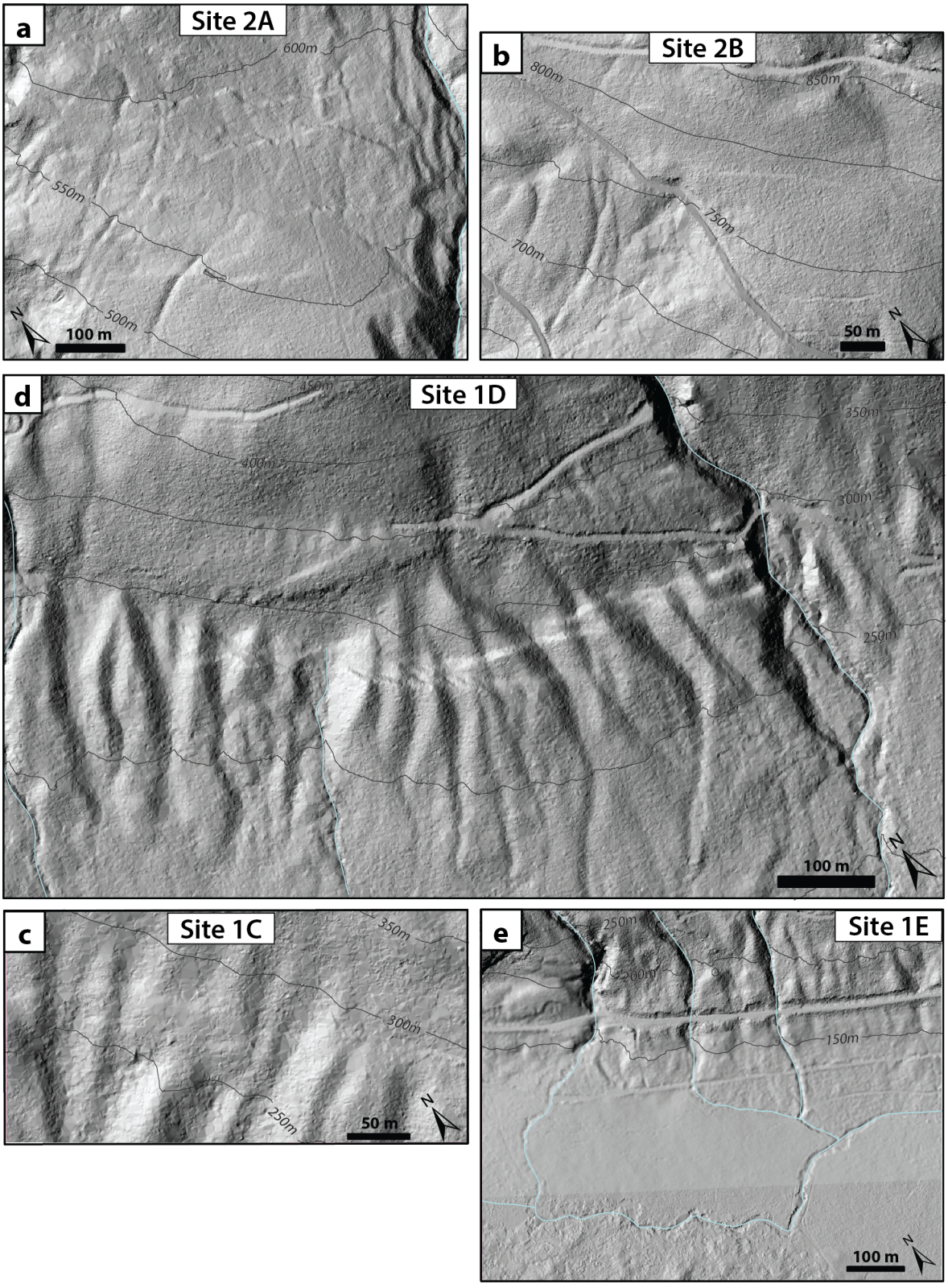

Figure S4. Unannotated versions of bare earth lidar DEMS for Sites 2A, 2B, 1C, 1D, and 1E.

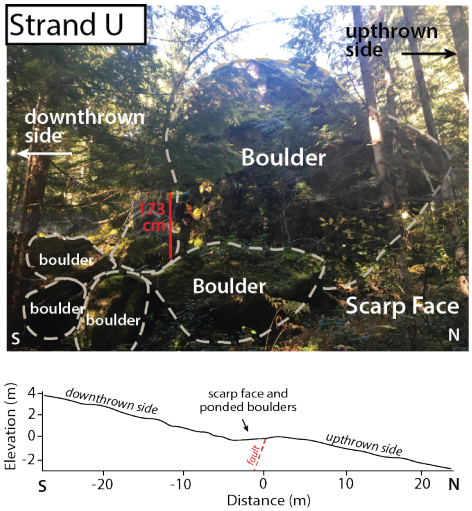

Figure S5. Field photos of a fault scarp (Strand U) at Site 2A. **A:** Photograph showing large boulders (∼1.5-8 m; outlined in dashed gray) ponded against fault scarp U at Site 2A. See main text Figures 4 and 6 for locations. **B:** Topographic profile across strand U.

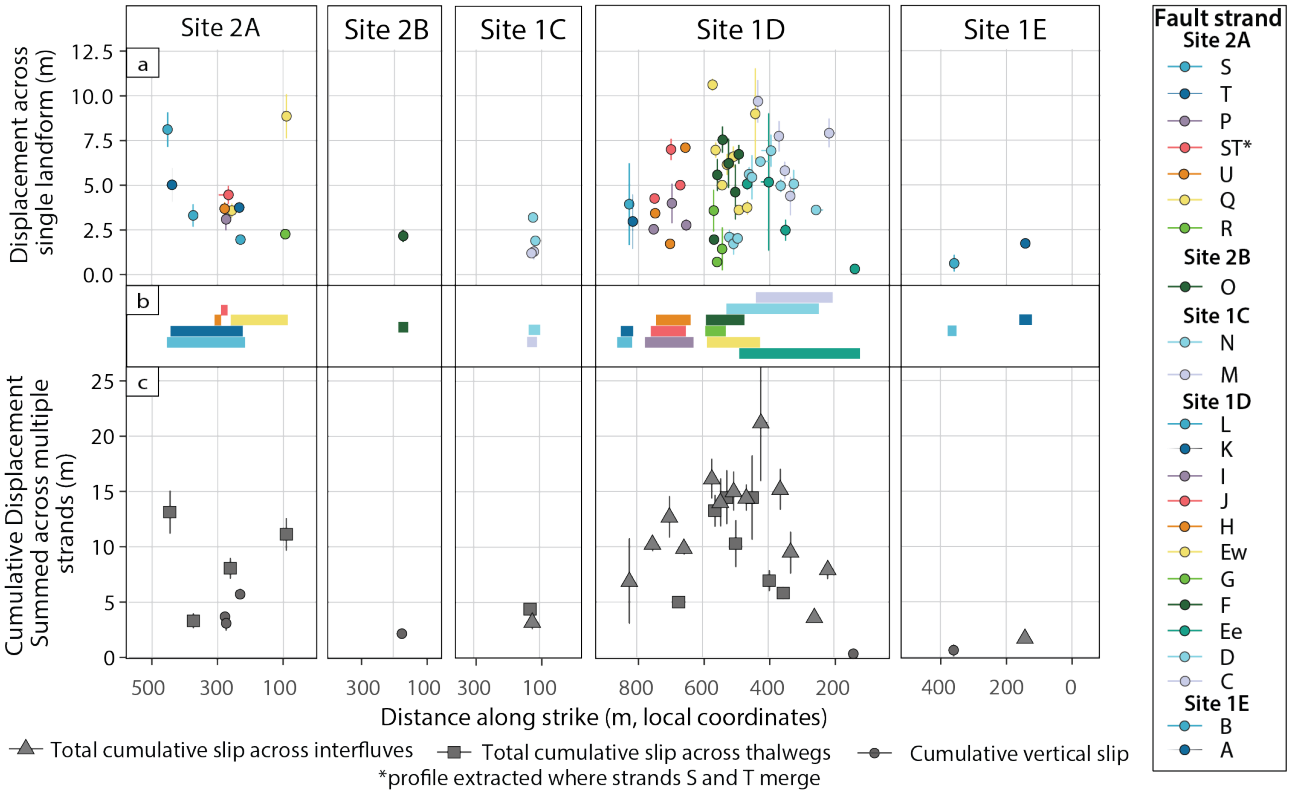

Figure S6. Displacement measured across the Beaufort Range fault at Sites A-E. Where error bars are not visible, the magnitude of error is smaller than the diameter of the symbol. **A:** Displacement of geomorphic landforms across individual fault strands (see Main Text Figure 7). Y axis error bars in panel c reflect 1 standard deviation calculated via a Monte Carlo simulation (see offset data in Table S2). **B:** Mapped extent of individual fault strands along strike (see detailed mapping in Main Text Figures 5 and 6). **C:** Cumulative displacement of geomorphic landforms summed across all surveyed fault strands. Error bars reflect the propagated sum of the errors on individual strands. Note that interfluve crests (triangles) show more displacement than channel thalwegs (squares). Straight-line profile (circles) do not capture any right-lateral displacement.

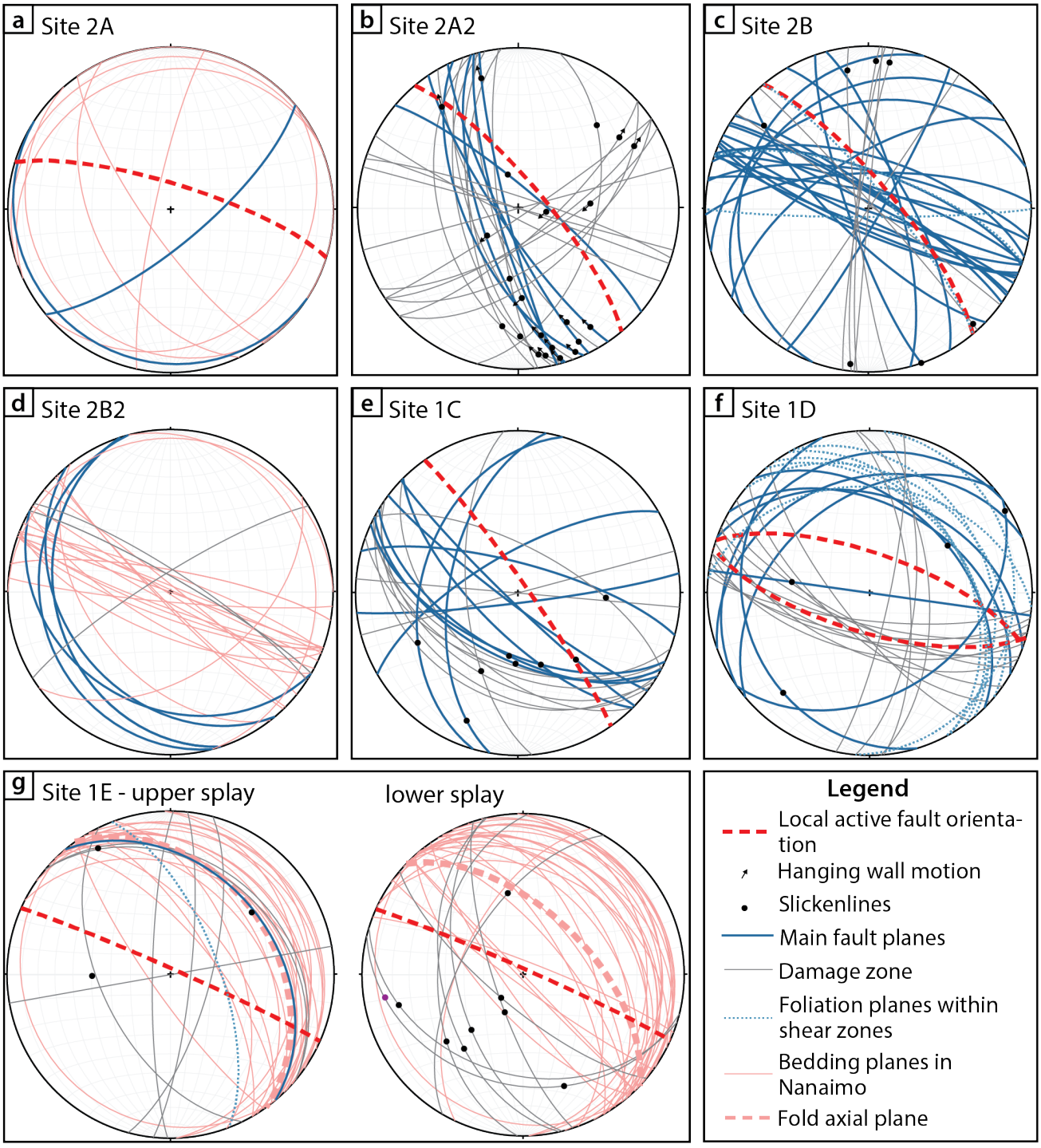

Figure S7. (Caption next page)

Figure S7. (Previous page). Lower hemisphere equal-area projections showing structural measurements in bedrock at Sites A-E (presented northwest to southeast; see Main Text Figure 4 and Figure S1 for locations). **A:** At Site 2A, bedrock faults and bedding planes are mostly gently dipping, in contrast with the active fault that is steeply dipping. Steeply-dipping bedding at this site is part of the upturned limb of a syncline in the footwall of the Eocene bedrock thrust fault. **B:** At Site 2A2, bedrock fault planes have similar dip magnitudes to the active fault, but opposite dip directions. Slickenlines and Riedel shear orientations (light gray) at Site 2A2 primarily record right-lateral, northeast-up motion. **C:** At Site 2B, the majority of bedrock fault planes are $\sim$20° oblique to the active fault strike. **D:** Site 2B2 is an exposure of Nanaimo bedding in a footwall syncline. **E:** At Site 1C, bedrock fault planes primarily dip southwest, and strikes are >10° apart from the active fault orientation. **F:** Site 1D records gently-dipping foliation and main bedrock fault planes, in contrast to steeply-dipping active fault planes. **G:** Site 1E records two footwall synclines in Nanaimo Fm., related to the two splays of the Eocene bedrock thrust fault (see Main Text Figure 4b).

Table S3. Nodal planes and P- and T-axis orientations for the 1946 Vancouver Island earthquake, and for kinematic inversions of BRF displacement data.

Solution	**Nodal Plane 1 (strike/dip)**	**Nodal Plane 2 (strike/dip)**	**P-axis (trend/plunge)**	**T-axis (trend/plunge)**	**Slip vector (trend/plunge)**[a]
1946 focal mechanism A[b]	319/79 NE	228/85 N	183/12	274/05	183/05
1946 focal mechanism B[b]	332/66 NE	233/70 NW	191/32	283/02	143/20
1946 focal mechanism C[b]	330/67 NE	222/36 NW	198/58	080/17	114/54
Site 2A[c]	276/78 N	181/64 W	141/27	046/09	096/10
Site 1C[c]	321/75 NE	199/26 NW	204/54	068/27	135/26
Site 2D[c]	292/66 NE	160/34 SW	165/61	040/17	107/15
Site 2E[c]	294/75 NE	187/43 W	164/45	053/20	109/19
All Sites[c]	296/83 NE	199/43 NW	170/37	058/26	109/48

[a] Calculated slip vector along NW-SE striking plane

[b] Focal mechanism solutions for the 1946 Vancouver Island earthquake (Rogers and Hasegawa, 1978)

[c] FaultKin inversions for the Beaufort Range fault, from offset piercing lines, this study